Received: 25 October 2024 | Revised: 14 February 2025 | Accepted: 16 February 2025

DOI: 10.1002/alz.70091

Alzheimer's & Dementia®
THE JOURNAL OF THE ALZHEIMER'S ASSOCIATION

RESEARCH ARTICLE

Intraneuronal Aβ accumulation causes tau hyperphosphorylation via endolysosomal leakage

Yang Gao[1] | Lisha Wang[1] | Tosca Doeswijk[1] | Bengt Winblad[1,2] | Sophia Schedin-Weiss[1] | Lars O. Tjernberg[1]

[1]Division of Neurogeriatrics, Department of Neurobiology, Care Sciences and Society, Karolinska Institutet, Solna, Sweden

[2]Theme Inflammation and Aging, Karolinska University Hospital, Huddinge, Sweden

Correspondence
Lars O. Tjernberg, Division of Neurogeriatrics, Department of Neurobiology, Care Sciences and Society, Karolinska Institutet, 171 64 Solna, Sweden.
Email: lars.tjernberg@ki.se

Funding information
Margaretha af Ugglas´ Foundation; Swedish Alzheimer's Foundation; China Scholarship Council; Stiftelsen för Gamla Tjänarinnor; Gun och Bertil Stohnes Stiftelse; Swedish Research Council

Abstract

INTRODUCTION: Alzheimer's disease (AD) is characterized by amyloid beta (Aβ) peptide plaques and intracellular neurofibrillary tangles formed by hyperphosphorylated tau. Many attempts have been made to clarify the link between Aβ and tau in the pathogenesis, but conclusive data describing a pathway for this connection are still lacking.

METHODS: We developed a neuronal model of Aβ-induced toxicity and studied downstream effects of intraneuronal Aβ42 accumulation on tau hyperphosphorylation using confocal microscopy and live cell imaging.

RESULTS: Aβ42 added to the medium was endocytosed into neurons, inducing the formation of endolysosomal protofibrils and endolysosomal leakage, which in turn promoted tau hyperphosphorylation. Asparaginyl endopeptidase (AEP) was released from the disrupted lysosomes, and inhibition of this peptidase activity reduced tau hyperphosphorylation.

DISCUSSION: The data suggest a mechanism of AD in which Aβ42 accumulates and aggregates gradually in neurons over time, leading to endolysosomal leakage and release of AEP, which subsequently triggers tau hyperphosphorylation.

KEYWORDS
Alzheimer's disease, amyloid beta peptide, asparaginyl endopeptidase, endolysosomal leakage, tau hyperphosphorylation

Highlights

- Aβ42 endocytosis leads to its endolysosomal accumulation in neurons over time.
- Aβ42 polymerizes into protofibrils and causes endolysosomal leakage.
- Tau hyperphosphorylation is induced by endolysosomal asparagine endopeptidase leakage.
- Tau hyperphosphorylation is inhibited by an asparagine endopeptidase inhibitor.

1 | BACKGROUND

Alzheimer's disease (AD) is a progressive neurodegenerative disease, pathologically characterized by neurofibrillary tangles and amyloid plaques in the brain parenchyma. Amyloid plaques consist of fibrils formed by the amyloid beta (Aβ) peptide – especially the 42 residues long variant (Aβ42). The neurofibrillary tangles, on the other hand, are formed by hyperphosphorylated forms of the microtubule-associated protein tau. The amyloid cascade hypothesis[1,2] suggests that AD starts with Aβ oligomerization, leading to plaque formation, neurofibrillary tangles, inflammation, oxidative stress, and eventually synaptic loss and death of neurons. This hypothesis has been challenged,[3–7] but the success of anti-Aβ immunotherapy lends further support to the notion that Aβ is a crucial player in AD pathogenesis.[8] Nevertheless, fundamental questions persist.

Post mortem examination of brain tissue has shown that Aβ42 accumulates in neurons at early stages of AD and before tangles are observed.[9–14] Studies in living neurons have shown that they efficiently endocytose Aβ, suggesting that the extracellular pool may be an important source of Aβ42 accumulation in neurons.[15,16] Previously we found that Aβ42 reaches high concentrations in endolysosomes (referring to late endosomes and lysosomes), where it oligomerizes.[16] Such Aβ aggregates are known to disrupt lipid membranes,[17,18] potentially compromising membrane integrity and leading to endolysosomal leakage.

Tau phosphorylation status depends largely on protein phosphatase 2A (PP2A) activity, which is regulated by inhibitor 2 of phosphatase protein 2A (I_2PP2A). The inhibitory effect of I_2PP2A is activated upon proteolytic processing mediated by asparaginyl endopeptidase (AEP), which is activated in lysosomes.[19] Thus, one question is how AEP translocates to the cytosol. To this end, we hypothesized that the accumulation and aggregation of Aβ42 would disrupt endolysosomes and release AEP to the cytoplasm. This results in increased processing of I_2PP2A, generating fragments that inhibit PP2A and, thus, eventually lead to increased tau hyperphosphorylation. To test this hypothesis, we used a galectin-based system to visualize Aβ42-induced endolysosomal leakage in neurons and demonstrated the release of endolysosomal AEP from damaged endolysosomes. We found that endolysosomal leakage induced tau hyperphosphorylation, which was diminished by AEP inhibition. Thus, we propose a potential mechanism for how intraneuronal Aβ42 accumulation causes tau hyperphosphorylation in AD.

RESEARCH IN CONTEXT

1. **Systematic review**: The authors reviewed the literature using traditional sources like PubMed. Although extensive research has been conducted on the role of Aβ in AD, the connection between Aβ and tau in AD pathogenesis remains unclear.
2. **Interpretation**: Our findings led to an integrated hypothesis explaining Aβ-triggered tau hyperphosphorylation in AD. This hypothesis is consistent with current neuropathological findings in AD patients and mouse models.
3. **Future directions**: Future studies should investigate the relationship between lysosomal Aβ aggregation and lysosomal leakage. Revealing the underlying mechanisms of lysosomal Aβ toxicity could help in developing novel therapeutic strategies to reduce tau hyperphosphorylation in AD.

2 | METHODS

2.1 | Synthetic human Aβ peptide

Aβ42 with or without a fluorescence label (AS-64161, AS-60479-01, AS-20276) and fluorescently labeled Aβ40 (AS-60493) were from AnaSpec (BioNordika, Solna, Sweden). Aβ peptides were first dissolved in 1% NH_4OH and diluted with PBS to a concentration of 200 µM, then aliquoted and stored at −20°C.

2.2 | Primary neuron cultures

This study was approved by the Linköping ethics committee (ID 1241, 16334-2022). Primary hippocampal neurons were prepared from embryonic brains of E16.5 C57/BL6 mice or E17.5 Sprague Dawley rats, as described previously.[20,21] After dissection and trituration of the cells from the hippocampal and cortical regions, 7500 hippocampal neurons were plated on the glass bottoms of poly-D-lysine-coated dishes (P35G-1.5-10-C, MatTek Corporation), and 150,000 cortical neurons were seeded at the pre-coated edges of the dishes as a support layer. Neurons were fed with neurobasal medium (Invitrogen) containing 2% B27 (Invitrogen) and 1% L-glutamine (Invitrogen) and put in a humidified cell incubator (37°C, 5% CO_2).

For immunoblotting, primary neurons were prepared from the embryonic brains of E16.5 C57/BL6 mice. After dissection and trituration of the cells from the cortical region, 8×10^5 cells per well were plated on the poly-D-lysine-coated six-well plate. For fractionation of lysosomes, 5×10^6 cells were plated on the poly-D-lysine-coated 150-mm dishes. Neurons were cultured as described earlier.

2.3 | Light microscopy

For different purposes, we employed three light microscopy platforms as described in what follows. The detailed information of image acquisition is shown in Table S1.

Platform 1 involved lattice light-sheet microscopy. For live cell imaging to monitor the uptake of fluorescently labeled Aβ42 into neurons co-stained with cytoskeletal markers, time-lapse images were acquired with a ZEISS Lattice Light-sheet 7 microscope (Advanced Light Microscopy facility, SciLifeLab) with an integrated cell incubator. Platform 2 involved single-point scanning confocal microscopy. For

time-lapse images of fluorescently labeled Aβ42 and lysosomes, images were acquired with a Nikon A1 Plus confocal microscope (Live Cell Imaging core facility, Karolinska Institutet) equipped with a stage incubator. Platform 3 employed confocal laser scanning microscopy with Airyscan. Live cell imaging at high resolution was performed with a Zeiss LSM 980-Airy confocal microscope (Biomedicum Imaging Core, Karolinska Institutet) equipped with a stage incubator.

2.4 | Live cell labeling

SiR-Lysosome (SC012, Spirochrome AG) was used to label endolysosomes in live cell imaging at a concentration of 1 μM for 0.5 h, unless otherwise specified. For time-lapse imaging, neurons were treated with 100 nM SiR-Lysosome for 6 h. SiR-Tubulin (SC002, Spirochrome AG) was used to label the cytoskeleton in time-lapse imaging (100 nM, 12 h).

2.5 | Volume measurement of neuronal vesicles

To measure the volume of neuronal soma and Aβ42-containing vesicles, neurons were treated with 1 nM HF647-Aβ42 for 3 weeks. Alexa Fluor 555-dextran was added just before live cell imaging. Z-stack images of neuronal soma were acquired by platform 3 and analyzed in ImageJ with macro code from Dr. Thomas Villani.[22]

2.6 | Transfection and transduction

Primary neurons were transfected using Lipofectamine 2000 (Invitrogen) at DIV 7-14. Transfection solutions were prepared according to the manufacturer's instructions. To save transfection reagents, excess medium in the neuronal culture dishes was removed and stored in a 37°C incubator; 500 μL of medium was left in the outside layer and 100 μL in the center microwell. Fresh neurobasal medium with 25 to 100 ng DNA, and 0.4 μL transfection reagent was added to the microwell for 4 h, then stored medium was added back and incubated for 24 to 48 h before use.

Primary neurons were transduced with CellLight Late Endosome-GFP (C10588, Invitrogen) or Premo Autophagy Sensor LC3B-GFP (P36235, Invitrogen) at a final concentration of 7.5 particles per cell. The neurons were incubated for 24 to 48 h before use.

2.7 | Model of endolysosomal leakage

Endolysosomal leakage in primary neurons was induced using L-leucyl-L-leucine methyl ester (LLOMe) (16008, Cayman Chemical) or Aβ42 at different conditions, as indicated. For the treatment of Aβ42-induced endolysosomal leakage, Aβ42 was applied through two separate sessions to keep the neurons viable. For example, a 10-h treatment was split into two 5-h sessions on two consecutive days. For the galectin puncta assay analyzed using live cell imaging, neurons were transfected with pEGFP-hGal3, which was a gift from Tamotsu Yoshimori (Addgene plasmid no. 73080).[23] For the galectin puncta assay and the ESCRT puncta assay analyzed using immunocytochemistry, neurons were stained with galectin-3 (GAL3) and CHMP5 antibodies (Table S2). For the fluorescent dextran release assay, neurons were treated with 30 μg/mL Alexa Fluor 555-dextran, 10 kDa (D34679, Invitrogen) 24 h before experiments.

2.8 | Immunocytochemistry

Immunocytochemistry procedures were described previously.[24] Primary neurons were fixed with preheated 4% formaldehyde in neurobasal medium (10 min). Fixed neurons were permeabilized using 0.4% CHAPSO at room temperature for 10 min. Neurons were blocked with 10% normal goat serum, or 10% donkey serum if primary antibodies were raised in goat (room temperature, 15min), and then incubated with primary antibodies in 3% normal goat or donkey serum in PBS, overnight at 4°C. After washing with PBS, neurons were incubated with secondary antibodies in 3% normal goat or donkey serum in PBS for 1 h at room temperature. For AT8 staining, the incubation time with secondary antibodies was shortened to 20 min. Samples were rinsed three times in PBS prior to imaging. Antibodies used here are listed in Table S2.

2.9 | Immunoblotting

DIV15 neurons were incubated with or without AENK (40 μg/mL) for 48 h following a 4-day treatment of 2 μM Aβ42. At DIV21, neurons were lysed in RIPA buffer (20-188, Millipore) supplemented with 2% SDS and protease and phosphatase inhibitor cocktail (PPC1010, Sigma). After centrifugation (20,000 × g, 4°C, 20 min), supernatants were collected and analyzed by Western blot. Protein concentrations were determined using the BCA protein assay kit (23235, Thermo Fisher Scientific). Protein samples were separated on the NuPAGE 4% to 12% Bis-Tris gel (NP0321, Invitrogen) and transferred to nitrocellulose membranes (88018, Thermo Fisher Scientific). The membranes were then blocked with 5% milk for 1 h at room temperature and probed with the following antibodies: anti-phospho-tau (AT8, Ser202, and Thr205, 1:1000 dilution, MN1020, Invitrogen), anti-phospho-tau (Thr217, 1:1000 dilution, 44-744, Invitrogen), anti-tau (clone tau5, 1:1000 dilution, MAB361, Merk), and anti-β-actin (1:3000 dilution, A2103, Sigma) primary antibodies overnight at 4°C. After washing three times with TBST (1×), membranes were incubated with IRDye donkey anti-mouse or anti-rabbit secondary antibody (1:10,000 dilution, LI-COR) for 1 h at room temperature protected from light. After washing with TBST (1×), the protein bands were visualized by the Odyssey CLx imaging system (LI-COR) and quantified using ImageJ version 1.53.

2.10 | Measurements of fluorophore concentration

Confocal microscopy was used to estimate the intravesicular Aβ42 concentration in neuronal culture.[25] To make a standard curve between the fluorescence intensity and the fluorescence concentration, the intensity of known concentrations of fluorophore HiLyte Fluor 647 was measured. HiLyte Fluor 647 amine (AS-81257, AnaSpec) was dissolved in double-distilled water to prepare evenly distributed solutions, and to the microwell of culture dishes (described earlier) was added 60-μL samples at different concentrations. Confocal microscopy (platform 3) was used to measure the fluorescence intensity of the samples. Images were taken from each sample at 2 μm above the bottom. Bottom levels were determined under confocal live mode (bright field, 0.2% 488 nm laser power, 300 V detector gain) by adjusting focus until the marks on the glass become sharp and clear. Intensities were measured by Zeiss Software Zen 3.0 (Carl Zeiss). A standard curve of fluorescence intensities against concentrations of HiLyte Fluor 647 was plotted using GraphPad Prism 8.3.0. For the estimation of the concentrations of HiLyte Fluor 647 Aβ42 in live neurons, the parameters of image acquisition were the same as the measurement for HiLyte Fluor 647.

2.11 | Image analysis

To measure the intensity of fluorescently labeled Aβ42, images acquired from platform 1 were processed using maximal intensity Z projection. Soma regions of neurons were outlined, and the intensity was measured in Zen 3.0. For images from platform 2, regions of neuronal soma were outlined, and the intensity was measured in ImageJ 1.53. For high-resolution images from platform 3, the fluorescence intensity in vesicles was measured in Zen 3.0.

For the galectin puncta assay, neurons were stained for GAL3 and RAB7 and imaged by platform 3. Soma regions of neurons were outlined, and the intensity was measured in Zen 3.0. To determine GAL3-positive endolysosomes, the colocalization analysis of GAL3 and RAB7 was performed to generate images containing only vesicles with colocalized signals. The vesicles with GAL3 were further detected using the ImageJ plugin TrackMate.[26]

To analyze the contents of AEP in neuronal lysosomes, neurons were stained with AEP and MAP2. Z-stack images of the entire soma region of neurons in five fields of view from each group were acquired by confocal microscope (platform 3) and processed to generate orthogonal projection images by Zen 3.0 using maximum-intensity Z projection. The ImageJ plugin TrackMate was used to detect the vesicles containing AEP with intensities above threshold.

To evaluate tau hyperphosphorylation, neurons were stained with AT8 antibody and imaged by confocal microscopy. Tau hyperphosphorylation was defined as excessive AT8 signal in the soma compared with that in controls. Abnormal AT8 signal was determined using the "Analyze Particles" plugin in ImageJ. The threshold was set to the highest values of AT8 intensities in the neuronal soma of controls. Neuron survival was determined by the number of MAP2-stained neurons in the views of images.

2.12 | Lysosome isolation

DIV14 neurons were incubated with or without treatment of 1 μM Aβ42 for 7 days. At DIV21, neurons were used for lysosome isolation. According to the procedures from the manufacturer, lysosome enrichment was performed using a lysosome enrichment kit for cultured cells (Catalog No. 89839, Pierce). In brief, TrypLE Express (12604021, Gibco) was used to detach the cells from dishes. Cells (1×10^7) were harvested by a centrifugation (300 × g, 5 min), and cell pellets were homogenized on ice using a Dounce grinder (15 to 30 strokes). Then a density gradient centrifugation (145,000 × g, 2 h, 4°C) was performed, and the obtained lysosome band was further purified through centrifugation.

Three microliter of purified lysosome solution was applied to the EM gold grid (N1-C14nAu20-01, QUANTIFOIL) and blotted using a Vitrobot Mark IV cryo fixation system (Thermo Fisher Scientific) at 4°C and 100% humidity (blot time 8 s, blot force −18, drain time 1.5 s). Frozen grids were clipped into autogrids and stored in liquid nitrogen until use.

2.13 | Cryo-ET and image processing

Cryogenic electron tomography (cryo-ET) was performed using a 300-kV Krios G3i transmission-electron microscope (Thermo Fisher Scientific) at the 3D-EM facility of Karolinska Institutet. Cryo-ET images were acquired using Tomography software on a Gatan K3 camera operated in electron-counted/super resolution mode. Features of interest were identified in the images that were taken at magnifications 580× and 6500× and were selected for high-magnification imaging. Image series were collected with a tilt span of 60° (± 30° from the tilt angle; dose-symmetric scheme) with 2° increments at a magnification of 53,000× (with a corresponding pixel size of 1.7 Å) and a defocus target of −8 μm. The raw tomographic images were preprocessed for Contrast Transfer Function estimation in Warp 1.0,[27] aligned and reconstructed with SART reconstruction in AreTomo.[28] Measurements of protofibrils were made in IMOD 4.11.[29] Image denoising was performed using the DenoisEM plugin (Tikhonov denoising) for ImageJ,[30] and segmentations were made with the ImageJ plugin Labkit.[31]

2.14 | Statistics

GraphPad Prism 10.0 software was used to perform statistical tests and plot data. Figures were assembled using Adobe Illustrator (San Jose, California, USA). The statistical tests used are indicated in the figure legends. When the *p* value was greater than 0.05, it was stated as "ns" or its original value. *P* values of $^*p < .05$, $^{**}p < .01$, and $^{***}p < .001$ were considered significant.

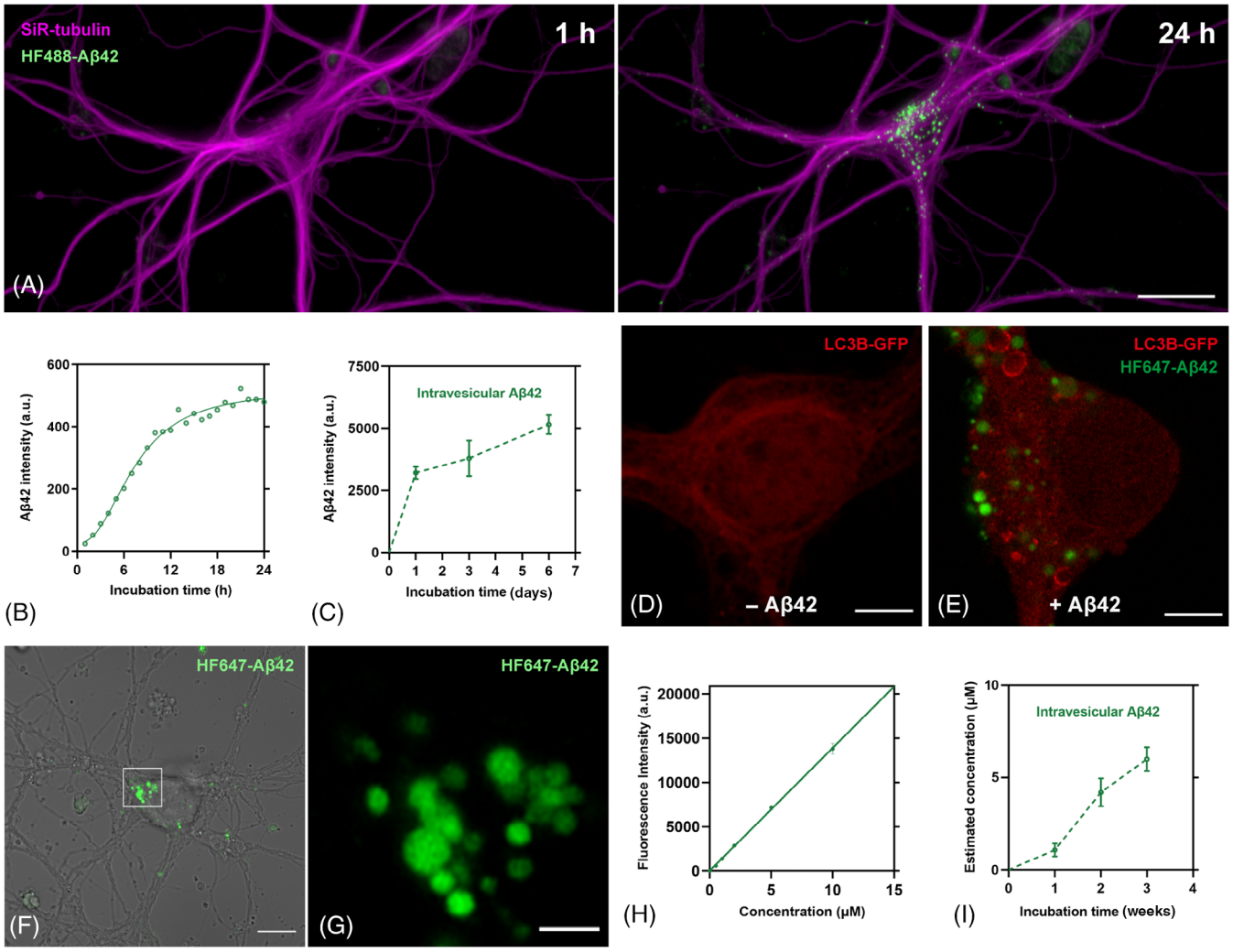

FIGURE 1 Aβ42 accumulation in primary neurons. (A and B) Hippocampal neurons treated with 1 μM HiLyte Fluor 488 Aβ42 (HF488-Aβ42, green) were imaged by live cell imaging using lattice light-sheet microscopy for 24 h. SiR-tubulin (violet) was used to label microtubules in neurons. Scale bar, 20 μm. The intensity of Aβ42 in the soma at different time points is plotted in (B). (C) Hippocampal neurons were treated with 1 μM HiLyte Fluor 647 Aβ42 for 1, 3, or 6 days and imaged using confocal microscopy. The intensity of Aβ42 in the neuronal vesicles (30, 39, and 27 vesicles from three experiments) were measured and plotted. Note that the intensity unit is arbitrary units and not comparable between the graphs. (D and E) Hippocampal neurons transduced with LC3B-GFP (red) were incubated without (D) or with (E) 1 μM HiLyte Fluor 647 Aβ42 (HF647-Aβ42, green) for 24 h and subjected to live cell imaging by confocal microscopy. Scale bar, 5 μm. (F–I) Hippocampal neurons were treated with 1 nM HiLyte Fluor 647 Aβ42 (HF647-Aβ42) for 3 weeks. (F) Confocal image merged with brightfield image showed accumulated HF647-Aβ42 (green) in the soma of neurons. Scale bar, 10 μm. (G) Magnification of the confocal channel for the boxed area in (F). Scale bar, 2 μm. (H) The fluorescence intensities of HiLyte Fluor 647 of different concentrations were measured by confocal microscopy and plotted to generate a standard curve ($n = 5$). (I) The fluorescence intensities of HF647-Aβ42 in neuronal vesicles (27 vesicles in each group from three experiments) were measured at weeks 1, 2, and 3. The concentrations of intravesicular Aβ42 were estimated based on the standard curve in (H). Data represent mean ± SD (C, H, and I). Aβ, amyloid β.

3 | RESULTS

3.1 | Endocytosed Aβ42 accumulates in endolysosomes of neurons

To study the endocytosis and accumulation of Aβ in neurons, we used lattice light-sheet microscopy and confocal microscopy to visualize the uptake of fluorescently labeled Aβ42 in primary neurons. During the time-lapse imaging, internalized Aβ42 was trafficked in vesicles – partially through neurites – and accumulated gradually in the soma (Figure 1A and Video S1). The concentration of intracellular Aβ42 rapidly rose in the first 12 h, followed by a slower increase in the subsequent days (Figure 1B, C). After 2 h of treatment, around 50% of Aβ42 was colocalized with the marker of early endosomes (Figure S1). After 24 h of treatment, around 90% of Aβ42 was present in endolysosomes (Video S2). These data suggest that endocytosed Aβ42 was initially

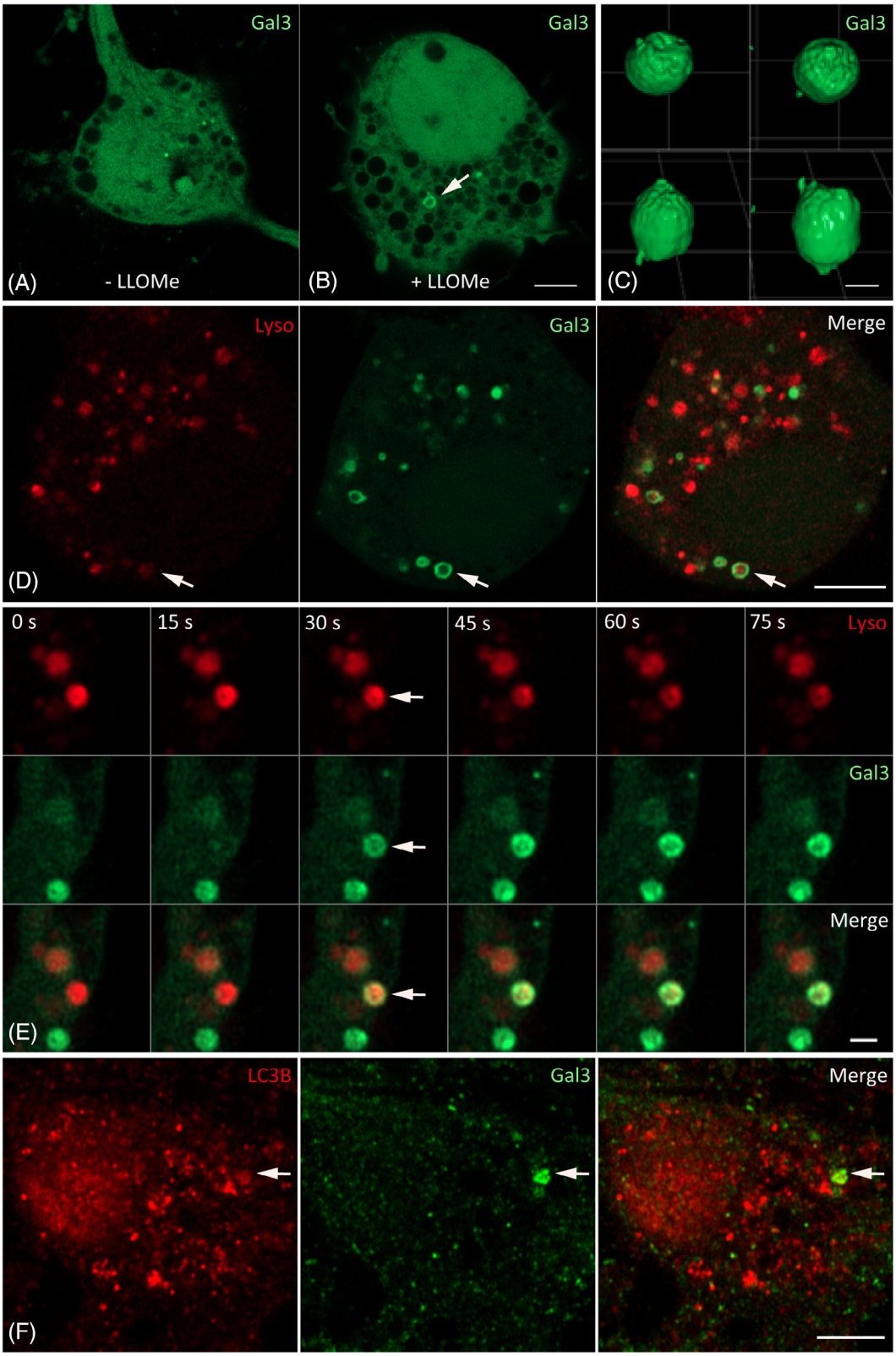

FIGURE 2 Galectin assay detects LLOMe-induced endolysosomal leakage in neurons. (A and B) Primary hippocampal neurons were transfected with pEGFP-hGal3 (Gal3, green) and then treated without (A) or with (B) 2 mM LLOMe for 2 h before live cell imaging. The arrow in (B) points to a leaky endolysosome. (C) 3D views of ruptured endolysosome in rat hippocampal neurons treated with LLOMe. (D) Primary rat hippocampal neurons were transfected with pEGFP-hGal3 and incubated with SiR-lysosome (lyso, red) for 1 h, followed by incubation with 2 mM LLOMe for 2 h. The arrow points to a leaky endolysosome, which is characterized by strong pEGFP-hGal3 staining but weak signal of SiR-lysosome.

present in the early endosomes and then gradually accumulated in the endolysosomes. Moreover, Aβ42 treatment increased the amount of LC3B-positive autophagosomes. However, only a limited amount of Aβ42 was present in these vesicles (Figure 1D, E).

The concentration of Aβ42 in human cerebrospinal fluid is in the nanomolar range.[32–34] To determine whether extracellular Aβ42 could be endocytosed at such low concentrations, neurons were treated with 1 nM fluorescently labeled Aβ42 for 3 weeks. Indeed, Aβ42 was internalized into endolysosomes with high efficiency even at such low concentrations (Figure 1F–G, Figure S2). Fluorescence intensity analysis, based on a standard curve generated from known concentrations of HiLyte Fluor 647 (Figure 1H), suggested that the concentration of intravesicular Aβ42 increased at an average rate of ~300 nM/day and reached micromolar levels in 1 week (Figure 1I). In comparison, the accumulation of Aβ40 in neurons was significantly lower than that of Aβ42 (Figure S3). In addition, volume measurements from confocal image stacks showed that Aβ42-containing vesicles occupied about 4% of the volume of neuronal soma (Figure S4).

3.2 | Detection of endolysosomal leakage in primary neurons

Since Aβ42 accumulated to concentrations well above the threshold for Aβ42 aggregation,[35] we investigated whether the high load of Aβ would damage the endolysosomes. LLOMe rapidly accumulates in the lumen of acidified organelles and permeabilizes membranes within 10 min,[36] making it an ideal tool to study endolysosomal damage. As a positive control for endosomal leakage, we treated the cells with fluorescent dextran – which accumulates in endolysosomes – and added LLOMe to the medium. A significant LLOMe-induced leakage of dextran from endolysosomes was observed (Figure S5A).

Next, we used the galectin puncta assay to detect endolysosomal leakage in neurons.[37] GAL3 is a sugar-binding protein that quickly accumulates at the inner leaflet of ruptured vesicles, making it a sensitive tool to detect endolysosomal leakage. Primary neurons transfected with GAL3 with an EGFP tag (pEGFP-hGal3) were treated with LLOMe to induce endolysosomal leakage. Instead of the diffuse cytosolic signal in untreated neurons, vesicle-shaped galectin signal appeared in LLOMe-treated neurons, indicating a rupture of endolysosomes (Figure 2A–D). Live cell imaging captured the rupture of an intact lysosome (Figure 2E and Video S3). Interestingly, a few GAL3-positive vesicles were colocalized with the autophagy marker LC3B, in line with previous studies on lysosomal leakage,[37,38] indicating that a group of leaky endolysosomes were subjected to autophagy/lysophagy (Figure 2F). To verify that the transfection did not affect the results, neurons were treated with LLOMe and stained with GAL3 antibody. LLOMe treatment induced endolysosomal leakage in non-transfected cells (Figure S5B).

3.3 | Aβ42 accumulation induces endolysosomal leakage

Using the galectin puncta assay, we studied whether accumulation of Aβ42 damaged the integrity of neuronal endolysosomes. The transfection-based galectin system was applied in neurons at 7 to 14 days in vitro (DIV7-14). In neurons transfected with GFP-GAL3, we observed Aβ42-induced endolysosomal leakage (Figures 3A and 3B). The concentration of Aβ42 in intact vesicles can reach around 100 μM or higher before endolysosomal leakage is induced (Figure S6A). Aβ42-induced endolysosomal leakage was further confirmed in mature neurons (DIV21) using a GAL3 antibody (Figures 3C and 3D). The number of disrupted endolysosomes increased when neurons were treated with a higher concentration of Aβ42 for a longer time (Figures 3E and 3F). Aβ42 treatment also increased the number of GAL3-positive endolysosomes in LLOMe-treated neurons (Figure S6B). Similarly to the results from LLOMe treatment, a group of leaky endolysosomes was co-stained with LC3B, indicating that Aβ42-induced endolysosomal leakage could induce autophagy (Figure S6C). Furthermore, the dextran release assay also demonstrated Aβ42-induced endolysosomal leakage (Figure S7). Interestingly, Aβ42 could be released from ruptured vesicles before the release of lysosomal enzymes (Figure S8).

Next, we used the ESCRT puncta assay, which efficiently detects small endolysosomal ruptures.[39] Unlike galectins that enter disrupted vesicles, ESCRT-III proteins (CHMP1-7) can accumulate on the cytoplasmic surface of ruptured vesicles. Consistent with previous findings in the AD brain,[40] ESCRT-III proteins formed puncta in Aβ42-treated neurons (Figures 3G and 3H).

3.4 | Aβ42 induces tau hyperphosphorylation through endolysosomal AEP leakage

AEP is a lysosomal enzyme that has been shown to translocate from lysosomes to the cytoplasm in AD brains and to be associated with tau hyperphosphorylation.[19] To investigate whether Aβ42 induces translocation of AEP from lysosome, neurons were treated with Aβ42 to induce intracellular Aβ42 accumulation. Endolysosomal AEP alterations were evaluated using immunocytochemistry. High concentrations of Aβ42, as well as LLOMe treatment, significantly decreased the number of AEP-containing endolysosomes (Figures 4A–D). In line with these results, AEP was not present in Aβ42-induced leaky

(E) Time-lapse images show the process of endolysosomal leakage in rat hippocampal neurons under the same condition as in (D). The arrow points to a leaky endolysosome, where the pEGFP-hGal3 enters and accumulates rapidly, while the signal of SiR-lysosome decreases over time. (F) Primary rat hippocampal neurons treated with LLOMe and stained for LC3B (red) and galectin-3 (Gal3, green). Scale bar, 5 μm (A, B, D, and F) and 1 μm (C and E). GAL3, galectin-3; LLOMe, L-leucyl-L-leucine methyl ester.

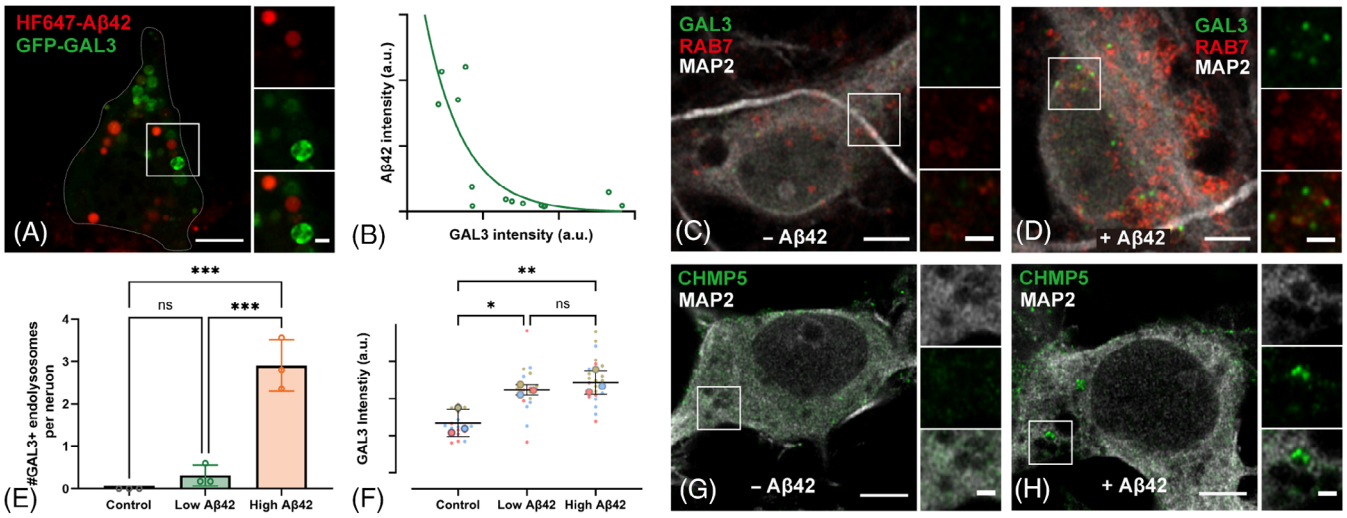

FIGURE 3 Accumulated Aβ42 induces endolysosomal leakage in neurons. (A) Primary neurons transfected with GFP-GAL3 (green) were treated with 1 μM HiLyte Fluor 647 Aβ42 (HF647-Aβ42, red) for 24 h. Vesicles with strong GFP-GAL3 signal indicate ruptured lysosomes. The intensities of HF647-Aβ42 versus GFP-GAL3 of the vesicles are plotted in (B). A non-linear curve was generated to fit the intensity data of the vesicles. (C–F) Primary neurons without treatment (C), treated with 1 μM Aβ42 for 24 h (Low Aβ42), with 5 μM Aβ42 for 48 h (High Aβ42) (D) were stained for MAP2, GAL3, and endolysosomes (RAB7). GAL3-positive lysosomes were defined as GAL3 puncta colocalized with RAB7 staining. The numbers of GAL3-positive lysosomes (in 19, 17, and 25 neurons from three experiments) are shown in (E). The intensities of GAL3 in the soma of those neurons are plotted in (F). The intensity of each cell is represented by a small dot, and values from three independent experiments are shown in different colors. Large dots represent global fractions per experiment. Statistical test, one-way ANOVA; data represent mean ± SD. (G and H) Primary neurons were treated with (H) or without (G) 5 μM Aβ42 for 24 h and stained with MAP2 (white) and ESCRT-III protein CHMP5 (green). Scale bar, 5 μm (1 μm in inset). Aβ, amyloid beta; GAL3, galectin-3.

endolysosomes (Figure 4D). These data together suggest that Aβ42 induces translocation of AEP from lysosomal lumen to the cytosol.

Since the cleavage of I_2PP2A by AEP inhibits PP2A and upregulates tau phosphorylation,[19] we examined whether AEP leakage could cause tau hyperphosphorylation. Neurons were treated with Aβ42 or LLOMe to induce AEP leakage, and tau phosphorylation was quantified by immunocytochemistry and Western blot (Figure 4E). Aβ42 and LLOMe treatment resulted in tau hyperphosphorylation, which was alleviated by an AEP inhibitor (AENK), indicating that tau hyperphosphorylation was dependent on AEP activity (Figure 4F–K, Figures S9 and S10). As expected, endolysosomal leakage was shown to be present in neurons with tau hyperphosphorylation (Figure S11). Neuronal survival was not affected by Aβ42 treatment, while LLOMe treatment slightly reduced survival rates (Figures 4H and 4K). Further analysis revealed that longer durations of LLOMe treatment led to an increased number of neurons with hyperphosphorylated tau (Figure 4L). In summary, these data suggest that Aβ42-induced AEP leakage can cause tau hyperphosphorylation.

3.5 | Aβ42 protofibril structure in neuronal lysosomes

Confocal images showed that the amount of Aβ42 in lysosomes increased with incubation time (Figure S12), and it is known that Aβ42 can form oligomers in neuronal endolysosomes.[16] To reveal the morphology of these oligomers and their potential involvement in lysosomal leakage, we isolated lysosomes from neurons by ultracentrifugation and performed cryo-ET. Under cryo-electron microscope, lysosomes from Aβ42-treated neurons displayed higher density than controls, with some exhibiting increased size and deformations (Figure S13). Cryo-ET images further revealed distinct morphological features of Aβ42 aggregates in Aβ42-treated lysosomes (Figure 5A–D). Notably, no protofibrils were observed in lysosomes from untreated cells (Figure S13). The most notable features are the protofibrils,[41,42] which appear as short fibrils less than 200 nm in length and approximately 8 to 13 nm in width, located near the membrane in some lysosomes (Figure 5E and 5F). In many cases, it appears that protofibrils arise from high-density granules, which could be oligomers or fragmented fibrils (Figure 5G–J). A few protofibrils tended to protrude outside the membrane, indicating that they might rupture the membrane (Figure 5K–N).

4 | DISCUSSION

The connection between Aβ and tau in AD pathogenesis has not been fully characterized. Here we show that Aβ42 is endocytosed by neurons and accumulates over time in endolysosomes. The endocytosed Aβ42 could be monomeric, oligomeric, or aggregated. Importantly, the accumulation and aggregation of Aβ42 induce the rupture of the endolysosomal membrane, resulting in leakage of the endolysosomal

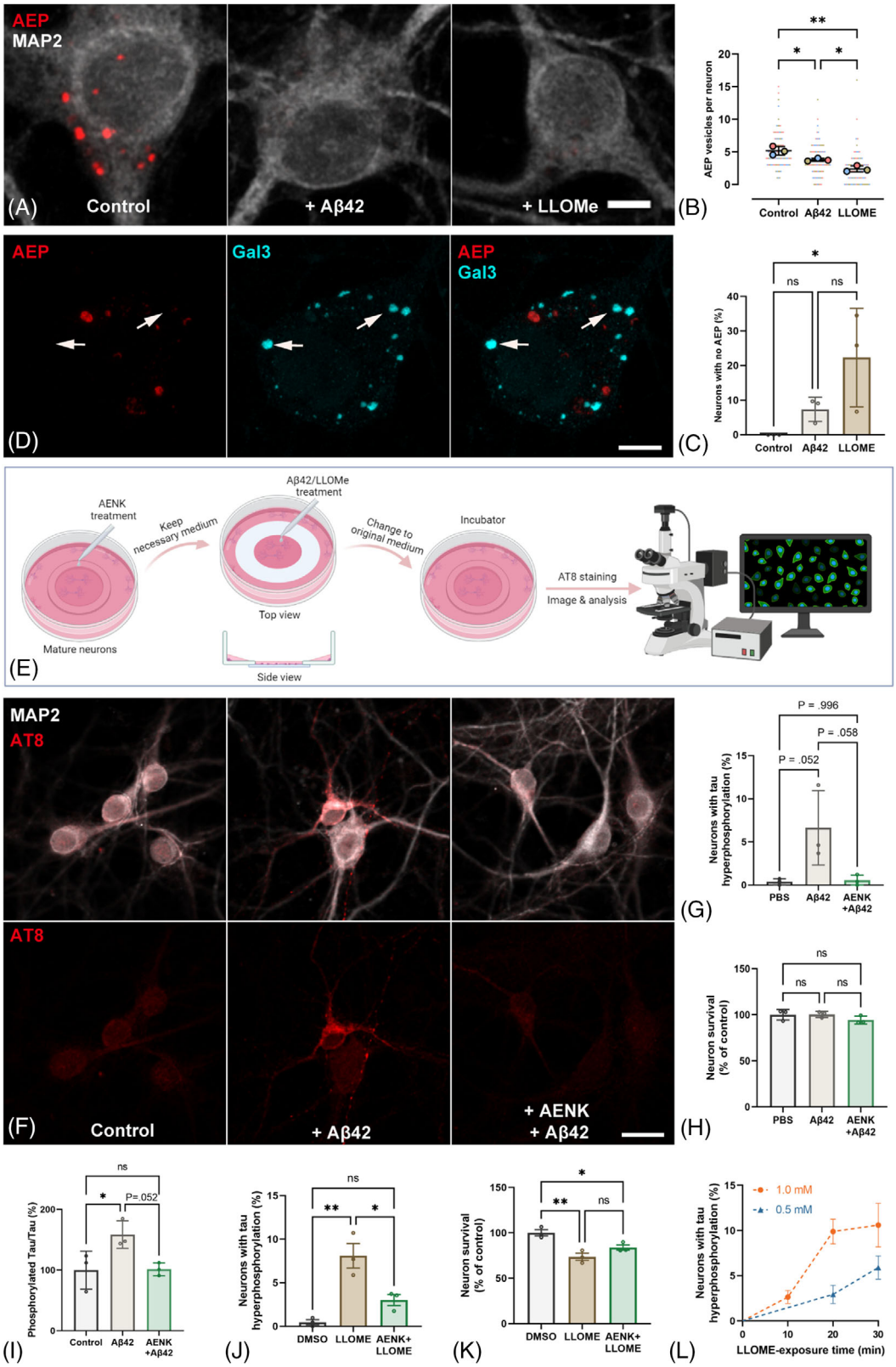

FIGURE 4 Endolysosomal AEP leakage induces tau hyperphosphorylation. (A) Primary neurons were treated with 1 mM LLOMe for 30 min or 25 μM Aβ42 for 10 h and stained for AEP and MAP2. Confocal images of representative neurons with or without endolysosomal AEP leakage are shown. Scale bar, 5 μm. The numbers of AEP-positive vesicles (in 102, 94, and 90 neurons from three independent experiments) are plotted in (B). The percentages of neurons without AEP-positive vesicles are shown in (C). (D) Confocal images of Aβ42-treated neurons treated with 25 μM Aβ42 for 10 h and stained with GAL3 and AEP. GAL3-positive vesicles (arrows) indicate ruptured endolysosomes where AEP staining is absent. Scale bar, 5 μm. (E) Schematic illustration of setup for studying endolysosomal leakage-induced tau hyperphosphorylation in neurons treated with

AEP inhibitor AENK (40 μg/mL), Aβ42 (25 μM), or LLOMe (1 mM). Neurons were treated with Aβ42 or LLOMe to induce endolysosomal AEP leakage. After treatment, neurons were incubated with only medium for 5 days, stained for AT8 and MAP2, and evaluated for tau phosphorylation. (F–H) Primary neurons were incubated with AENK for 48 h and then incubated with 25 μM Aβ42 for a further 10 h (as described in E). The representative confocal images are shown in (F). Scale bar, 20 μm. The percentages of neurons with tau hyperphosphorylation (G) and neuron survival (H) of three groups were plotted (from three independent experiments). (I) Primary neurons were incubated with or without AENK (40 μg/mL) for 48 h following a 4-day treatment of 2 μM Aβ42. Phosphorylated tau (AT8) and total tau (tau5) in cell lysate were detected by Western blot, and the p-tau/tau ratio was quantified. (J and K) Primary neurons were incubated with AENK for 48 h following the treatment of LLOMe for 15 min (as described in E). The percentage of neurons with tau hyperphosphorylation (J) and neuron survival (K) (from three independent experiments). (L) Primary neurons were incubated with LLOMe at indicated conditions and evaluated for tau phosphorylation. Statistical test, one-way ANOVA; data represent mean ± SD. Aβ, amyloid beta; AEP, asparaginyl endopeptidase; GAL3, galectin-3; LLOMe, L-leucyl-L-leucine methyl ester.

content, including AEP, to the cytosol. Thus, AEP mislocalized to the cytosol generates I_2PP2A fragments, which inhibit PP2A and thereby promote tau hyperphosphorylation.

In neuronal culture, we replicate the pathological features observed in neurons of the AD brain (Figure 6). The neurons are exposed to external Aβ42 to induce pathological Aβ42 accumulation and aggregation, further resulting in endolysosomal leakage. Crucially, the neuron model reproduces the translocation of AEP and tau hyperphosphorylation, as seen in AD. The accumulation of Aβ42 in endolysosomes that we observed in primary mouse hippocampal neurons is similar to the situation in the human brain. The Aβ42 concentration in hippocampal neurons in the AD brain is five times higher, around 3 μM, than in the control brain and correlates with AD neuropathology.[9,10] Importantly, Aβ42 has been suggested to predominantly accumulate in the endolysosomal system also in AD brains.[43,44] Assuming that all Aβ42 is located in the endolysosomes, which occupy approximately

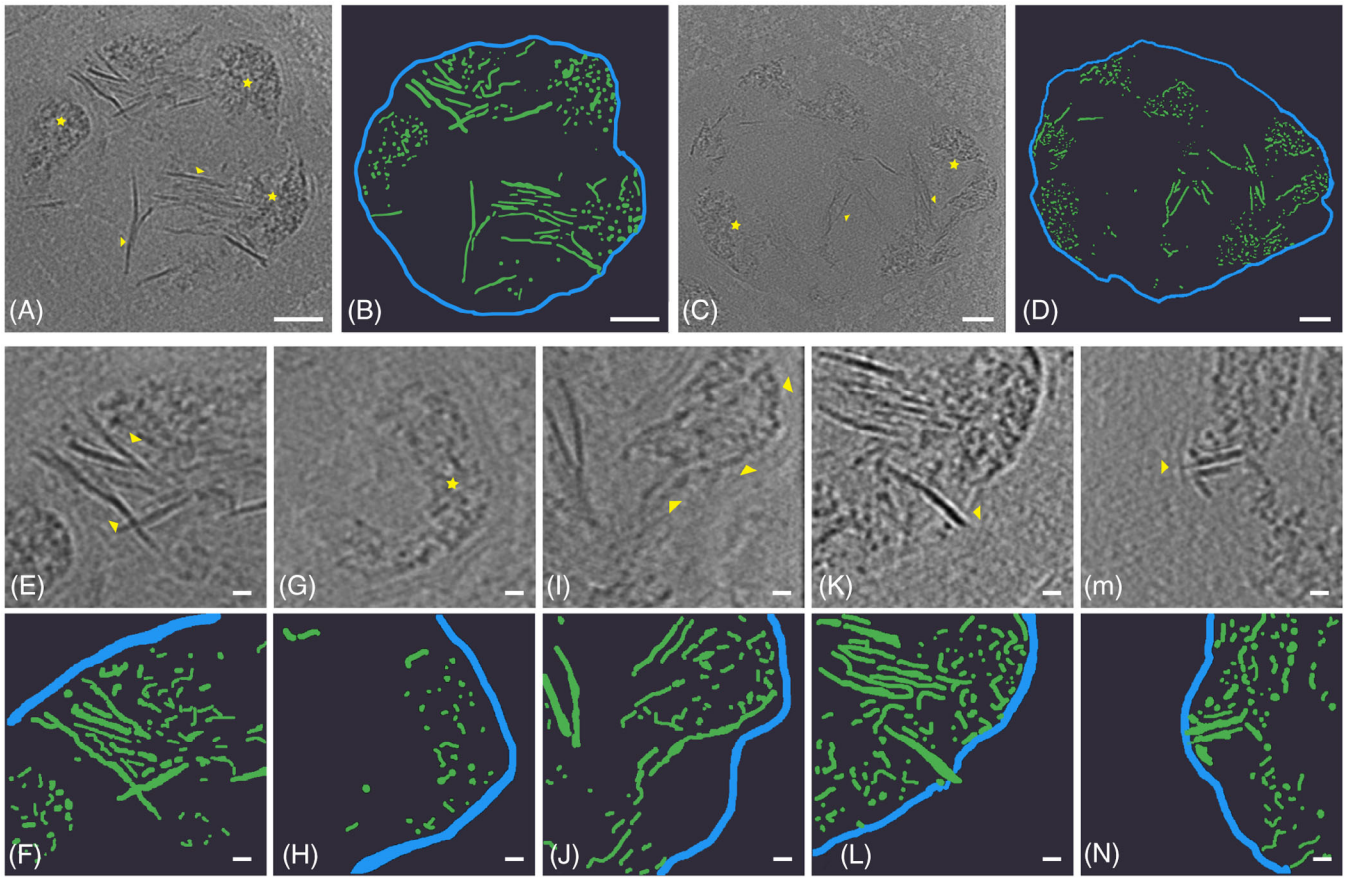

FIGURE 5 Aβ42 protofibrils in lysosomes of Aβ42-treated neurons. Isolated lysosomes of Aβ42-treated neurons were examined with cryo-ET. (A and C) Tomographic slices show the protofibrils (arrowheads) and granular aggregates (stars) present in lysosomes. (B and D) Segmentation views of tomogram in (A) and (C). (E–H) Protofibrils (arrowheads) and granular aggregates (stars). (I and J) Protofibrils (arrowheads) extend from the high-density granules (K–N). Protofibrils (arrowheads) tend to protrude outside the membrane. Scale bar, 100 nm (A–D), 20 nm (E–N). Aβ, amyloid beta; cryo-ET, cryo-electron tomography.

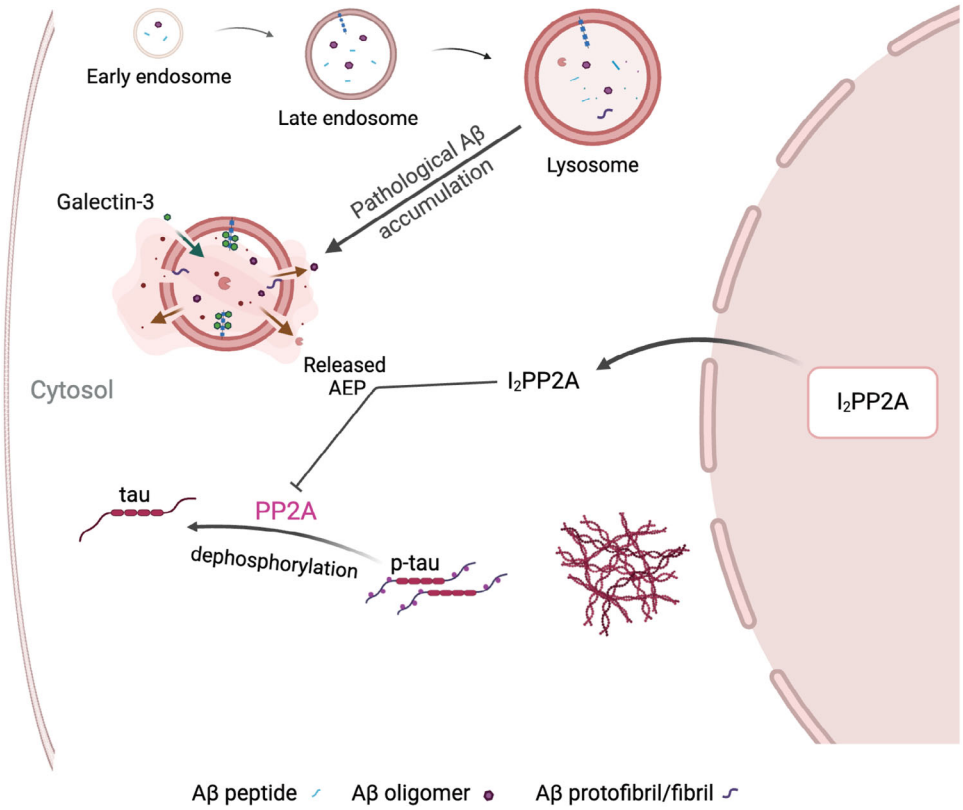

FIGURE 6 Potential mechanism for how Aβ42 induces tau hyperphosphorylation via lysosomal leakage. Aβ42 accumulates over time in neuronal endolysosomes and eventually damages the endolysosomal system. Ruptured endolysosomes release AEP, which cleaves I_2PP2A. Cleavage products from I_2PP2A inhibit PP2A, resulting in tau hyperphosphorylation and neurofibrillary tangles. Created with BioRender.com. Aβ, amyloid beta; AEP, asparaginyl endopeptidase; I_2PP2A, inhibitor-2 of phosphatase protein 2A.

4% of the soma volume, the average intravesicular Aβ42 concentration would be around 75 μM. Moreover, our observations suggest that Aβ42 is unevenly distributed among endolysosomes, potentially leading to concentrations of endolysosomal Aβ42 in AD brains reaching over 100 μM in some lysosomes. Such a high amount of Aβ42 leads to aggregation and endolysosomal leakage, and this might explain the findings of lysosomal leakage in AD brains.[40,45–48]

Determining the structures formed upon Aβ42 polymerization within the lysosome might help clarify the mechanisms behind Aβ42-induced lysosomal leakage. We previously used live cell Förster resonance energy transfer (FRET) imaging to demonstrate that Aβ42 polymerizes into aggregates in neuronal lysosomes.[16] Here we used cryo-ET and revealed that those lysosomal Aβ42 aggregates were, at least partially, protofibrils. Aβ protofibrils are known to disrupt lipid membranes.[17,18] Based on these results, we suggest that interactions between Aβ42 protofibrils and membranes rupture the lysosomal membrane. Thus, inhibiting Aβ42 aggregation in the lysosomes could be a treatment strategy for AD.

The endolysosomal integrity is crucial for the cell, and polymerization of compounds within the endolysosomal lumen – as exemplified by LLOMe[49] – may have detrimental effects. Thus, luminal/extracellular proteins or peptides present at high concentrations and with a strong tendency to polymerize may induce such leakage. To this end, Aβ42 is one of the most aggregation-prone peptides known, and it is expressed at relatively high levels in the human brain.[10] Thus, a minor increase in Aβ42 levels over time results in endolysosomal accumulation, polymerization, and endolysosomal leakage. This may in turn induce tau hyperphosphorylation due to inhibition of PP2A, eventually resulting in neuronal death.[19] Potentially, similar mechanisms may be involved in other neurodegenerative diseases,[50,51] but other mechanisms could cause similar effects.[52]

As will be discussed in what follows, reducing the polymerization of tau has been a therapeutic goal for decades.[53] Tau polymerization is highly dependent on its degree of phosphorylation – highly phosphorylated tau polymerizes into neurofibrillary tangles – and so kinases such as glycogen synthase kinase-3 (GSK3) have been targeted.[54] These attempts have not been fruitful, and more specific targeting of hyperphosphorylated tau is necessary. To this end, several antibodies directed to tau are undergoing clinical trials.[52] This strategy also seems problematic since tau is a cytosolic protein and not easily accessible to extracellular antibodies. It has been suggested that tau oligomers could propagate from neuron to neuron via exosomes and that the spread of tau pathology could be reduced by targeting such exosomes.[55] In neither case would tau be readily accessible to antibodies since it is contained within vesicles. Therefore, exploring approaches beyond direct tau targeting may be preferable.

Alternatively, targeting the processes that lead to tau phosphorylation could be effective for early pharmaceutical intervention. In AD,

certain neurons – such as the pyramidal cells in the hippocampus – contain high levels of Aβ42 and are more vulnerable than others.[9,10] According to this study, such high Aβ42 levels cause lysosomal leakage, which in turn results in tau phosphorylation. Thus, reducing Aβ42 uptake in these neurons would reduce tau hyperphosphorylation and concomitant tau pathology. However, there is a multitude of different receptors suggested to be involved in Aβ endocytosis.[56] Thus, targeting receptor-mediated Aβ42 uptake may be a complicated task. We have observed that Aβ42 is taken up by neurons more quickly than Aβ40 and that Aβ42 can oligomerize at the cell surface of neurons.[16] Hence, it is possible that both the C-terminus and degree of oligomerization affect the uptake, further complicating the possibility of reducing Aβ42 uptake.

Another approach to reducing tau hyperphosphorylation caused by lysosomal leakage is to inhibit lysosomal Aβ42 aggregation. This can be achieved by employing molecules that are delivered to lysosomes. The feasibility of this approach is supported by studies on the Bri2 protein, which has been shown to cross the blood–brain barrier and ameliorate the AD-like symptoms in mouse models.[57] Importantly, Bri2 is endocytosed by neurons and ends up in lysosomes, where it inhibits Aβ aggregation (unpublished data). From a pharmaceutical perspective, small organic molecules are an attractive alternative to proteins, and many low-molecular-weight compounds have shown anti-amyloidogenic properties.[58] Thus, delivering these compounds specifically to endolysosomes could provide organelle-specific targeting of Aβ polymerization. This targeted delivery could be achieved, for instance, by nanoparticles.[59]

In addition, AEP indirectly inhibits PP2A, thereby inducing hyperphosphorylated tau.[19] Thus, reducing AEP activity, as shown in this study using AENK, could be a pharmacological strategy aimed at reducing toxic forms of tau. Recent studies have shown that AEP inhibitors could reduce the toxic tau fragment both in vitro and in vivo, suggesting AEP inhibition may be a feasible and promising therapeutic strategy for AD.[60–62] To reduce potential side effects, a cytosolic inhibitor may be preferable since AEP plays a crucial role in lysosomal degradation.[63] Besides AEP, endolysosomal leakage might release other proteases (e.g., cathepsins), which may also affect tau phosphorylation and need further exploration.

In conclusion, we propose a potential mechanism for Aβ-triggered tau hyperphosphorylation in AD. In AD brains, Aβ42 accumulates pathologically in neuronal endolysosomes for decades, ultimately leading to endolysosomal damage. Leaked substances from endolysosomes like AEP would cause downstream events such as tau hyperphosphorylation in specific neuron populations. This mechanism not only aligns with current neuropathological findings in AD patients but also suggests novel pharmaceutical targets, thereby laying the groundwork for the development of innovative and effective AD therapies.

ACKNOWLEDGMENTS

The authors acknowledge technical support by Genis Valenti Gese, Amy Bondy, Martin Hällberg, and Thomas Thersleff (Karolinska Institutet). They acknowledge the National Microscopy Infrastructure (VR-RFI 2016-00968) and thank the Advanced Light Microscopy facility at Science for Life Laboratory, Stockholm, Sweden, for excellent support with lattice light-sheet microscopy. We thank the Live Cell Imaging facility, Karolinska Institutet, Sweden, supported by grants from the Knut and Alice Wallenberg Foundation, the Swedish Research Council, the Centre for Innovative Medicine and the Jonasson Centre at the Royal Institute of Technology, Sweden. This study received grants from Margaretha af Ugglas´ Foundation (B.W., S.S.-W.), Swedish Alzheimer's Foundation (L.O.T. and S.S.-W.), Swedish Research Council (L.O.T.), China Scholarship Council, Stiftelsen för Gamla Tjänarinnor, and the Gun and Bertil Stohnes Foundation.

CONFLICT OF INTEREST STATEMENT

The authors have no conflicts of interest to declare. Author disclosures are available in the supporting information.

CONSENT STATEMENT

A consent statement was not necessary.

ORCID

Yang Gao https://orcid.org/0000-0002-7733-5365
Lars O. Tjernberg https://orcid.org/0000-0001-6889-4950

REFERENCES

1. Hardy JA, Higgins GA. Alzheimer's disease: the amyloid cascade hypothesis. *Science*. 1992;256(5054):184-185. doi:10.1126/science.1566067
2. Wirths O, Multhaup G, Bayer TA. A modified beta-amyloid hypothesis: intraneuronal accumulation of the beta-amyloid peptide—the first step of a fatal cascade. *J Neurochem*. 2004;91(3):513-520. doi:10.1111/j.1471-4159.2004.02737.x
3. Caselli RJ, Knopman DS, Bu G. An agnostic reevaluation of the amyloid cascade hypothesis of Alzheimer's disease pathogenesis: the role of APP homeostasis. *Alzheimers Dement*. 2020;16(11):1582-1590. doi:10.1002/alz.12124
4. Herrup K. The case for rejecting the amyloid cascade hypothesis. *Nat Neurosci*. 2015;18(6):794-799. doi:10.1038/nn.4017
5. Barage SH, Sonawane KD. Amyloid cascade hypothesis: pathogenesis and therapeutic strategies in Alzheimer's disease. *Neuropeptides*. 2015;52:1-18. doi:10.1016/j.npep.2015.06.008
6. Karran E, De Strooper B. The amyloid cascade hypothesis: are we poised for success or failure?. *J Neurochem*. 2016;139(S2):237-252. doi:10.1111/jnc.13632
7. Ayton S, Bush AI. β-amyloid: the known unknowns. *Ageing Res Rev*. 2021;65:101212. doi:10.1016/j.arr.2020.101212
8. van Dyck CH, Swanson CJ, Aisen P, et al. Lecanemab in early Alzheimer's disease. *N Engl J Med*. 2023;388(1):9-21. doi:10.1056/NEJMoa2212948
9. Aoki M, Volkmann I, Tjernberg LO, Winblad B, Bogdanovic N. Amyloid β-peptide levels in laser capture microdissected cornu ammonis 1 pyramidal neurons of Alzheimer's brain. *NeuroReport*. 2008;19(11):1085-1089. doi:10.1097/WNR.0b013e328302c858
10. Hashimoto M, Bogdanovic N, Volkmann I, Aoki M, Winblad B, Tjernberg LO. Analysis of microdissected human neurons by a sensitive ELISA reveals a correlation between elevated intracellular concentrations of Abeta42 and Alzheimer's disease neuropathology. *Acta Neuropathol*. 2010;119(5):543-554. doi:10.1007/s00401-010-0661-6

11. Gouras GK, Tsai J, Naslund J, et al. Intraneuronal Aβ42 accumulation in human brain. *Am J Pathol*. 2000;156(1):15-20. doi:10.1016/S0002-9440(10)64700-1
12. Gouras GK, Tampellini D, Takahashi RH, Capetillo-Zarate E. Intraneuronal β-amyloid accumulation and synapse pathology in Alzheimer's disease. *Acta Neuropathol*. 2010;119(5):523-541. doi:10.1007/s00401-010-0679-9
13. Cabrejo L, Guyant-Maréchal L, Laquerrière A, et al. Phenotype associated with APP duplication in five families. *Brain*. 2006;129(11):2966-2976. doi:10.1093/brain/awl237
14. Wegiel J, Kuchna I, Nowicki K, et al. Intraneuronal Aβ immunoreactivity is not a predictor of brain amyloidosis-β or neurofibrillary degeneration. *Acta Neuropathol*. 2007;113(4):389-402. doi:10.1007/s00401-006-0191-4
15. Hu X, Crick SL, Bu G, Frieden C, Pappu RV, Lee JM. Amyloid seeds formed by cellular uptake, concentration, and aggregation of the amyloid-beta peptide. *PNAS*. 2009;106(48):20324-20329. doi:10.1073/pnas.0911281106
16. Gao Y, Wennmalm S, Winblad B, Schedin-Weiss S, LO Tjernberg. Live cell FRET imaging reveals amyloid β-peptide oligomerization in hippocampal neurons. *Int J Mol Sci*. 2021;22(9):4530. doi:10.3390/ijms22094530
17. Flagmeier P, De S, Michaels TCT, et al. Direct measurement of lipid membrane disruption connects kinetics and toxicity of Aβ42 aggregation. *Nat Struct Mol Biol*. 2020;27(10):886-891. doi:10.1038/s41594-020-0471-z
18. Kayed R, Sokolov Y, Edmonds B, et al. Permeabilization of lipid bilayers is a common conformation-dependent activity of soluble amyloid oligomers in protein misfolding diseases. *J Biol Chem*. 2004;279(45):46363-46366. doi:10.1074/jbc.C400260200
19. Basurto-Islas G, Grundke-Iqbal I, Tung YC, Liu F, Iqbal K. Activation of asparaginyl endopeptidase leads to tau hyperphosphorylation in Alzheimer disease. *J Biol Chem*. 2013;288(24):17495-17507. doi:10.1074/jbc.M112.446070
20. Fath T, Ke YD, Gunning P, Götz J, Ittner LM. Primary support cultures of hippocampal and substantia nigra neurons. *Nat Protoc*. 2009;4(1):78-85. doi:10.1038/nprot.2008.199
21. Thermo Fisher Scientific. Isolation, culture, and characterization of cortical and hippocampal neurons. Thermo Fisher Scientific; 2022. Accessed November 4, 2022. https://www.thermofisher.com/uk/en/home/references/protocols/neurobiology/neurobiology-protocols/isolation-culture-and-characterization-of-cortical-and-hippocampal-neurons.html
22. Villani T, Loading and measurement of volumes in 3D confocal image stacks with imageJ. Visikol; 2023. Accessed February 15, 2023. https://visikol.com/blog/2018/11/29/blog-post-loading-and-measurement-of-volumes-in-3d-confocal-image-stacks-with-imagej/
23. Maejima I, Takahashi A, Omori H, et al. Autophagy sequesters damaged lysosomes to control lysosomal biogenesis and kidney injury. *EMBO J*. 2013;32(17):2336-2347. doi:10.1038/emboj.2013.171
24. Yu Y, Gao Y, Winblad B, Tjernberg LO. Schedin-Weiss S. A super-resolved view of the Alzheimer's disease-related amyloidogenic pathway in hippocampal neurons. *J Alzheimers Dis*. 2021;83(2):833-852. doi:10.3233/JAD-215008
25. Fink C, Morgan F, Loew LM. Intracellular fluorescent probe concentrations by confocal microscopy. *Biophys J*. 1998;75(4):1648-1658. doi:10.1016/S0006-3495(98)77607-6
26. Ershov D, Phan MS, Pylvänäinen JW, et al. TrackMate 7: integrating state-of-the-art segmentation algorithms into tracking pipelines. *Nat Methods*. 2022;19(7):829-832. doi:10.1038/s41592-022-01507-1
27. Tegunov D, Cramer P. Real-time cryo-electron microscopy data preprocessing with warp. *Nat Methods*. 2019;16(11):1146-1152. doi:10.1038/s41592-019-0580-y
28. Zheng S, Wolff G, Greenan G, et al. AreTomo: an integrated software package for automated marker-free, motion-corrected cryo-electron tomographic alignment and reconstruction. *J Struct Biol X*. 2022;6:100068. doi:10.1016/j.yjsbx.2022.100068
29. Kremer JR, Mastronarde DN, McIntosh JR. Computer visualization of three-dimensional image data using IMOD. *J Struct Biol*. 1996;116(1):71-76. doi:10.1006/jsbi.1996.0013
30. Roels J, Vernaillen F, Kremer A, et al. An interactive ImageJ plugin for semi-automated image denoising in electron microscopy. *Nat Commun*. 2020;11(1):771. doi:10.1038/s41467-020-14529-0
31. Arzt M, Deschamps J, Schmied C, et al. LABKIT: labeling and segmentation toolkit for big image data. *Frontiers in Computer Science*. 2022;4:777728. doi:10.3389/fcomp.2022.777728
32. Lehmann S, Delaby C, Boursier G, et al. Relevance of Aβ42/40 ratio for detection of Alzheimer disease pathology in clinical routine: the PLMR scale. *Front Aging Neurosci*. 2018;10:138. https://www.frontiersin.org/articles/10.3389/fnagi.2018.00138
33. Janelidze S, Zetterberg H, Mattsson N, et al. CSF Aβ42/Aβ40 and Aβ42/Aβ38 ratios: better diagnostic markers of Alzheimer disease. *Ann Clin Transl Neurol*. 2016;3(3):154-165. doi:10.1002/acn3.274
34. Hansson O, Lehmann S, Otto M, Zetterberg H, Lewczuk P. Advantages and disadvantages of the use of the CSF amyloid β (Aβ) 42/40 ratio in the diagnosis of Alzheimer's disease. *Alzheimers Res Ther*. 2019;11(1):34. doi:10.1186/s13195-019-0485-0
35. Novo M, Freire S, Al-Soufi W. Critical aggregation concentration for the formation of early amyloid-β (1-42) oligomers. *Sci Rep*. 2018;8:1783. doi:10.1038/s41598-018-19961-3
36. Repnik U, Borg Distefano M, Speth MT, et al. L-leucyl-L-leucine methyl ester does not release cysteine cathepsins to the cytosol but inactivates them in transiently permeabilized lysosomes. *J Cell Sci*. 2017;130(18):3124-3140. doi:10.1242/jcs.204529
37. Aits S, Kricker J, Liu B, et al. Sensitive detection of lysosomal membrane permeabilization by lysosomal galectin puncta assay. *Autophagy*. 2015;11(8):1408-1424. doi:10.1080/15548627.2015.1063871
38. Eriksson I, Wäster P, Öllinger K. Restoration of lysosomal function after damage is accompanied by recycling of lysosomal membrane proteins. *Cell Death Dis*. 2020;11(5):1-16. doi:10.1038/s41419-020-2527-8
39. Skowyra ML, Schlesinger PH, Naismith TV, Hanson PI. Triggered recruitment of ESCRT machinery promotes endolysosomal repair. *Science*. 2018;360(6384):eaar5078. doi:10.1126/science.aar5078
40. Hondius DC, Koopmans F, Leistner C, et al. The proteome of granulovacuolar degeneration and neurofibrillary tangles in Alzheimer's disease. *Acta Neuropathol*. 2021;141(3):341-358. doi:10.1007/s00401-020-02261-4
41. Harper JD, Wong SS, Lieber CM, Lansbury PT. Observation of metastable Abeta amyloid protofibrils by atomic force microscopy. *Chem Biol*. 1997;4(2):119-125. doi:10.1016/s1074-5521(97)90255-6
42. Walsh DM, Lomakin A, Benedek GB, Condron MM, Teplow DB. Amyloid beta-protein fibrillogenesis. Detection of a protofibrillar intermediate. *J Biol Chem*. 1997;272(35):22364-22372. doi:10.1074/jbc.272.35.22364
43. Nixon RA, Mathews PM, Cataldo AM. The neuronal endosomal-lysosomal system in Alzheimer's disease. *J Alzheimers Dis*. 2001;3(1):97-107. doi:10.3233/jad-2001-3114
44. LaFerla FM, Green KN, Oddo S. Intracellular amyloid-β in Alzheimer's disease. *Nat Rev Neurosci*. 2007;8(7):499-509. doi:10.1038/nrn2168
45. Lee JH, Yang DS, Goulbourne CN, et al. Faulty autolysosome acidification in Alzheimer's disease mouse models induces autophagic build-up of Aβ in neurons, yielding senile plaques. *Nat Neurosci*. 2022;25(6):688-701. doi:10.1038/s41593-022-01084-8
46. Yamashima T, Oikawa S, The role of lysosomal rupture in neuronal death. *Prog Neurobiol*. 2009;89(4):343-358. doi:10.1016/j.pneurobio.2009.09.003

47. Adamec E, Mohan PS, Cataldo AM, Vonsattel JP, Nixon RA. Up-regulation of the lysosomal system in experimental models of neuronal injury: implications for Alzheimer's disease. *Neurosci*. 2000;100(3):663-675. doi:10.1016/S0306-4522(00)00281-5
48. Yang AJ, Chandswangbhuvana D, Margol L, Glabe CG. Loss of endosomal/lysosomal membrane impermeability is an early event in amyloid Aβ1-42 pathogenesis. *J Neurosci Res*. 1998;52(6):691-698.
49. Thiele DL, Lipsky PE. Mechanism of L-leucyl-L-leucine methyl ester-mediated killing of cytotoxic lymphocytes: dependence on a lysosomal thiol protease, dipeptidyl peptidase I, that is enriched in these cells. *Proc Natl Acad Sci U S A*. 1990;87(1):83-87.
50. Jiang P, Gan M, Yen SH, McLean PJ, Dickson DW. Impaired endo-lysosomal membrane integrity accelerates the seeding progression of α-synuclein aggregates. *Sci Rep*. 2017;7(1):7690. doi:10.1038/s41598-017-08149-w
51. Flavin WP, Bousset L, Green ZC, et al. Endocytic vesicle rupture is a conserved mechanism of cellular invasion by amyloid proteins. *Acta Neuropathol*. 2017;134(4):629-653. doi:10.1007/s00401-017-1722-x
52. Congdon EE, Ji C, Tetlow AM, Jiang Y, Sigurdsson EM. Tau-targeting therapies for Alzheimer disease: current status and future directions. *Nat Rev Neurol*. 2023;19(12):715-736. doi:10.1038/s41582-023-00883-2
53. Hanger DP, Anderton BH, Noble W. Tau phosphorylation: the therapeutic challenge for neurodegenerative disease. *Trends Mol Med*. 2009;15(3):112-119. doi:10.1016/j.molmed.2009.01.003
54. Basheer N, Smolek T, Hassan I, et al. Does modulation of tau hyperphosphorylation represent a reasonable therapeutic strategy for Alzheimer's disease? From preclinical studies to the clinical trials. *Mol Psychiatry*. 2023;28(6):2197-2214. doi:10.1038/s41380-023-02113-z
55. Jackson NA, Guerrero-Muñoz MJ, Castillo-Carranza DL. The prion-like transmission of tau oligomers via exosomes. *Front Aging Neurosci*. 2022;14:974414. doi:10.3389/fnagi.2022.974414
56. Yang G. *Alzheimer Disease: Subcellular Aβ Mechanisms and Treatment Strategies*. Karolinska Institutet; 2023. Accessed October 16, 2024. https://search.proquest.com/openview/a0ad11041053be3cc7fd00a38be30735/1?pq-origsite=gscholar&cbl=2026366&diss=y
57. Manchanda S, Galan-Acosta L, Abelein A, et al. Intravenous treatment with a molecular chaperone designed against β-amyloid toxicity improves Alzheimer's disease pathology in mouse models. *Mol Ther*. 2023;31(2):487-502. doi:10.1016/j.ymthe.2022.08.010
58. Salahuddin P, Khan RH, Furkan M, Uversky VN, Islam Z, Fatima MT. Mechanisms of amyloid proteins aggregation and their inhibition by antibodies, small molecule inhibitors, nano-particles and nano-bodies. *Int J Biol Macromol*. 2021;186:580-590. doi:10.1016/j.ijbiomac.2021.07.056
59. Shao X, Meng C, Song W, Zhang T, Chen Q. Subcellular visualization: organelle-specific targeted drug delivery and discovery. *Adv Drug Delivery Rev*. 2023;199:114977. doi:10.1016/j.addr.2023.114977
60. Krummenacher D, He W, Kuhn B, et al. Discovery of orally available and brain penetrant AEP inhibitors. *J Med Chem*. 2023;66(24):17026-17043. doi:10.1021/acs.jmedchem.3c01804
61. Qian Z, Li B, Meng X, et al. Inhibition of asparagine endopeptidase (AEP) effectively treats sporadic Alzheimer's disease in mice. *Neuropsychopharmacol*. 2024;49(3):620-630. doi:10.1038/s41386-023-01774-2
62. Zhang Z, Obianyo O, Dall E, et al. Inhibition of delta-secretase improves cognitive functions in mouse models of Alzheimer's disease. *Nat Commun*. 2017;8(1):14740. doi:10.1038/ncomms14740
63. Solberg R, Lunde NN, Forbord KM, Okla M, Kassem M, Jafari A. The mammalian cysteine protease legumain in health and disease. *Int J Mol Sci*. 2022;23(24):15983. doi:10.3390/ijms232415983

SUPPORTING INFORMATION

Additional supporting information can be found online in the Supporting Information section at the end of this article.

How to cite this article: Gao Y, Wang L, Doeswijk T, Winblad B, Schedin-Weiss S, Tjernberg LO. Intraneuronal Aβ accumulation causes tau hyperphosphorylation via endolysosomal leakage. *Alzheimer's Dement*. 2025;21:e70091. https://doi.org/10.1002/alz.70091